J Geod (2007) 81: 5–15
DOI 10.1007/s00190-006-0040-1

ORIGINAL ARTICLE

M. J. Fengler · W. Freeden · A. Kohlhaas
V. Michel · T. Peters

Wavelet modeling of regional and temporal variations of the earth's gravitational potential observed by GRACE

Received: 7 June 2005 / Accepted: 3 March 2006 / Published online: 8 July 2006

Abstract This work is dedicated to the wavelet modeling of regional and temporal variations of the Earth's gravitational potential observed by the GRACE (gravity recovery and climate experiment) satellite mission. In the first part, all required mathematical tools and methods involving spherical wavelets are provided. Then, we apply our method to monthly GRACE gravity fields. A strong seasonal signal can be identified, which is restricted to areas where large-scale redistributions of continental water mass are expected. This assumption is analyzed and verified by comparing the time-series of regionally obtained wavelet coefficients of the gravitational signal originating from hydrology models and the gravitational potential observed by GRACE. The results are in good agreement with previous studies and illustrate that wavelets are an appropriate tool to investigate regional effects in the Earth's gravitational field.

Keywords Spherical wavelets · GRACE (Gravity recovery and climate experiment) · Gravitational field · Hydrological gravity variations

1 Motivation

Over the last decade, wavelets have found important applications in numerous areas of mathematics, physics, engineering and computer science. Wavelets form versatile tools for representing general functions or data sets. They especially become more and more important in Earth sciences, since most recent satellite missions deliver millions of data scattered around the globe. Meanwhile, spherical wavelets introduced by Freeden and Schreiner (1995), Freeden and Windheuser (1996), Freeden et al. (1998), Freeden (1999) and further developments made from them play an important role in the analysis of regional, high-frequency phenomena observed in geophysical, geodetic, magnetic and meteorological applications (see e.g., Freeden 1999; Freeden and Michel 2004; Fengler et al. 2004a,b; Fengler 2005; Maier 2003; Mayer 2003 and many references therein).

The spherical wavelets discussed here are based on expansions in terms of Legendre polynomials. Hence, they form radial basis functions on the sphere, whose argument depends only on the spherical distance between the center of the wavelet and its evaluation point. In contrast to spherical harmonics, wavelets localize with respect to space. Wavelet coefficients depend also on space and not only on frequency such that regional changes do not influence the whole set of coefficients. Therefore, wavelets are an appropriate tool to filter regional signals. We want to highlight this by applying them to regional mass variations observed by the gravity recovery and climate experiment (GRACE) satellite mission (Tapley et al. 2004a).

The twin GRACE satellites have been in orbit for more than 3 years. A number of recent studies (e.g., Tapley et al. 2004b; Wahr et al. 2004; Andersen and Hinderer 2005; Han et al. 2005a; Rowlands et al. 2005) show that GRACE is capable of measuring large-scale mass redistributions within the Earth system. Most of the measured gravitational variations are believed to belong to hydrological mass redistributions, since other effects are corrected for (see Bettadpur 2003). Consequently, many studies of temporal variations in the gravitational field from GRACE are now focusing on the relationship between gravitational variations derived from hydrology models and the GRACE observations.

Hydrological mass redistributions are restricted to the continents. Hydrology models still have a poor performance in some areas due to the lack of observations, especially

Electronic Supplementary Material Supplementary materials is available to authorised users in the online version of this article at http://dx.doi.org/10.1007/s00190-006-0040-1

M. J. Fengler · W. Freeden (✉) · A. Kohlhaas · V. Michel
Department of Mathematics, Geomathematics Group,
University of Kaiserslautern, Kaiserslautern, Germany
E-mail: freeden@mathematik.uni-kl.de
Tel.: +49-631-2053867
Fax: +49-631-2054736

T. Peters
Technische Universität München,
Institut für Astronomische und Physikalische Geodäsie (IAPG),
München, Germany

in the polar regions. Therefore, a representation respecting the local character of the hydrological variations is desirable. Spherical harmonics are polynomials and, therefore, have a global support. Thus, if the gravity variations are represented in spherical harmonics, the erroneous information is smeared over the entire globe. Several approaches have been used to overcome this problem: Wahr et al. (1998), Ramillien et al. (2004), Tapley et al. (2004b), Andersen and Hinderer (2005) use a smoothing Gaussian filter proposed by Jekeli (1981), while Wahr et al. (2004) use special averaging kernels tailored to drainage basins and considering satellite errors and leakage errors (see Swenson and Wahr 2002; Swenson et al. 2003). Recently, Han et al. (2005a,b) and Rowlands et al. (2005) developed promising new techniques of gravity computation directly from the observed inter-satellite distances without using spherical harmonics.

The intention of our work is to present a method that can avoid the problems related to the global character of the spherical harmonics. We apply spherical wavelets to the spherical harmonic coefficients, which have been released as the so-called 'GRACE level 2 product', and to hydrology models given as gridded data. Hereby, wavelets are mathematically more appropriate for the analysis of regional mass variations. We exploit their strong localization, which means that local changes do not affect the whole potential but only certain regions. For instance, errors in the polar regions will not affect the equatorial region any more.

2 Preliminaries

In the following, we adopt the notation from Freeden et al. (1998). The letters $\mathbb{N}$, $\mathbb{N}_0$ and $\mathbb{R}$ denote the sets of positive integers, non-negative integers and real numbers, respectively. We write x, y to represent the elements of the three-dimensional Euclidean space $\mathbb{R}^3$ endowed with the Euclidean canonical basis $\{\varepsilon^1, \varepsilon^2, \varepsilon^3\}$. Then $x \cdot y = \sum_{i=1}^{3} x_i y_i$ is referred to as the canonical inner product. The corresponding norm is given by $|x| = \sqrt{x \cdot x}$. The unit sphere is represented by Ω; elements of it are usually given by ξ or η. Consequently, we denote by Ω_R the sphere of radius R, and its interior ball by Ω_R^{int}. As customary, the space of all real, square-integrable functions F on Ω is called $L^2(\Omega)$. $L^2(\Omega)$ is a Hilbert space with the inner product given by

$$\langle F, G\rangle_{L^2(\Omega)} = \int_{\Omega} F(\xi)G(\xi)\,\mathrm{d}S(\xi), \quad F, G \in L^2(\Omega), \tag{1}$$

and the associated norm

$$\|F\|_{L^2(\Omega)} = \left(\int_{\Omega} F^2(\xi)\,\mathrm{d}S(\xi)\right)^{1/2}, \quad F \in L^2(\Omega). \tag{2}$$

As is well known, the real-valued spherical harmonics $Y_{n,k}$ of degree n and order k form an orthonormal basis of $L^2(\Omega)$ (see, e.g., Edmonds 1964; Freeden et al. 1998). Hence, each $F \in L^2(\Omega)$ can be written uniquely in the $L^2(\Omega)$-sense in terms of a Fourier series, i.e.,

$$F = \sum_{n=0}^{\infty}\sum_{k=-n}^{n} F_{n,k}Y_{n,k}, \tag{3}$$

with

$$F_{n,k} = \int_{\Omega} F(\eta)Y_{n,k}(\eta)\,\mathrm{d}S(\eta). \tag{4}$$

As another important ingredient, we require the Legendre polynomials $t \mapsto P_n(t)$ of degree n which are, for instance, obtainable via the Rodriguez formula (e.g., Freeden et al. 1998)

$$P_n(t) = \frac{1}{2^n n!}\frac{\mathrm{d}^n}{\mathrm{d}t^n}(t^2-1)^n, \quad t \in [-1, 1]. \tag{5}$$

Altogether, we end up at the spherical addition theorem

$$\sum_{k=-n}^{n} Y_{n,k}(\xi)Y_{n,k}(\eta) = \frac{2n+1}{4\pi}P_n(\xi \cdot \eta) \tag{6}$$

connecting the spherical harmonics and the Legendre polynomials (see Freeden et al. 1998). As a matter of fact, Eq. (6) forms the foundation in formulating scaling functions and wavelets on the sphere.

Throughout this text, the notation $F(\xi, \cdot)$ is used for the function $\eta \mapsto F(\xi, \eta)$. From the context, no confusion should arise with the scalar product.

2.1 Scaling functions and wavelets

First, we require the so-called generator of a scaling function. The choice of this generator determines all properties of the scaling function and its associated wavelet:

A family $\{\{\Phi_J^\wedge(n)\}_{n\in\mathbb{N}_0}\}_{J\in\mathbb{N}_0}$ is called a generator of a scaling function, if it satisfies the following requirements:

1. for all $J \in \mathbb{N}_0$
$$(\Phi_J^\wedge(0))^2 = 1; \tag{7}$$
2. for all $J, J' \in \mathbb{N}_0$ with $J \le J'$ and all $n \in \mathbb{N}$
$$0 \le (\Phi_J^\wedge(n))^2 \le (\Phi_{J'}^\wedge(n))^2; \tag{8}$$
3. for all $n \in \mathbb{N}$
$$\lim_{J\to\infty}(\Phi_J^\wedge(n))^2 = 1. \tag{9}$$

For fixed $J \in \mathbb{N}_0$, the sequence $\{\Phi_J^\wedge(n)\}_{n\in\mathbb{N}_0}$ is called the *symbol* of the corresponding scaling function Φ_J of scale J. According to Freeden et al. (1998), this scaling function of scale J is defined by

$$\Phi_J(\xi, \eta) = \sum_{n=0}^{\infty}\Phi_J^\wedge(n)\frac{2n+1}{4\pi}P_n(\xi \cdot \eta). \tag{10}$$

Now, suppose that $\{\{\Phi_J^\wedge(n)\}_{n\in\mathbb{N}_0}\}_{J\in\mathbb{N}_0}$ is a generator of a scaling function. Then the families $\{\{\Psi_J^\wedge(n)\}_{n\in\mathbb{N}_0}\}_{J\in\mathbb{N}_0}$ and $\{\{\tilde{\Psi}_J^\wedge(n)\}_{n\in\mathbb{N}_0}\}_{J\in\mathbb{N}_0}$ are said to be the generators of the primal and the dual wavelet, respectively, if the *refinement equation*

$$\tilde{\Psi}_J^\wedge(n)\Psi_J^\wedge(n) = (\Phi_{J+1}^\wedge(n))^2 - (\Phi_J^\wedge(n))^2 \tag{11}$$

is satisfied for all $J \in \mathbb{N}_0$ and $n \in \mathbb{N}_0$. Consequently, the primal and dual wavelet of scale J, respectively, read as:

$$\Psi_J(\xi,\eta) = \sum_{n=0}^{\infty} \Psi_J^\wedge(n) \frac{2n+1}{4\pi} P_n(\xi\cdot\eta), \tag{12}$$

$$\tilde{\Psi}_J(\xi,\eta) = \sum_{n=0}^{\infty} \tilde{\Psi}_J^\wedge(n) \frac{2n+1}{4\pi} P_n(\xi\cdot\eta). \tag{13}$$

Since we consider only P-scale wavelets (see Freeden 1999) in this work, we simply let $\tilde{\Psi}_J^\wedge(n) = \Psi_J^\wedge(n)$, $J \in \mathbb{N}_0, n \in \mathbb{N}_0$. Hence, the symbol is computed by

$$\Psi_J^\wedge(n) = \sqrt{(\Phi_{J+1}^\wedge(n))^2 - (\Phi_J^\wedge(n))^2}. \tag{14}$$

Scaling function $\{\Phi_J\}_{J\in\mathbb{N}_0}$ and wavelet $\{\Psi_J\}_{J\in\mathbb{N}_0}$, respectively, are called *bandlimited* if the symbols $\{\Phi_J^\wedge(n)\}_{n\in\mathbb{N}_0}$ and $\{\Psi_J^\wedge(n)\}_{n\in\mathbb{N}_0}$, respectively, are for fixed scale J different from zero only for finitely many values of n. For an overview on the different types of scaling functions and wavelets, we refer to Freeden et al. (1998) and Freeden (1999).

In this work, we restrict ourselves to the consideration of scaling functions and wavelets generated by the so-called cubic polynomial (CuP) in the frequency domain, i.e., we let

$$\Phi_J^\wedge(n) = \begin{cases} (1-2^{-J}n)^2(1+2^{-J+1}n) & \text{for } n \in [0, 2^J), \\ 0 & \text{for } n \in [2^J, \infty), \end{cases} \tag{15}$$

from which one can verify that all three conditions of a generator are fulfilled. However, it should be remarked that every other generator satisfying Eqs. (7), (8) and (9) can also be taken into account. Finally, we should outline that the CuP scaling functions and wavelets are bandlimited, and possess a well-localizing shape in the space domain, (see Figs. 1, 2). Note that we present the radial basis functions in dependency of the angle θ between ξ and η. The corresponding symbols

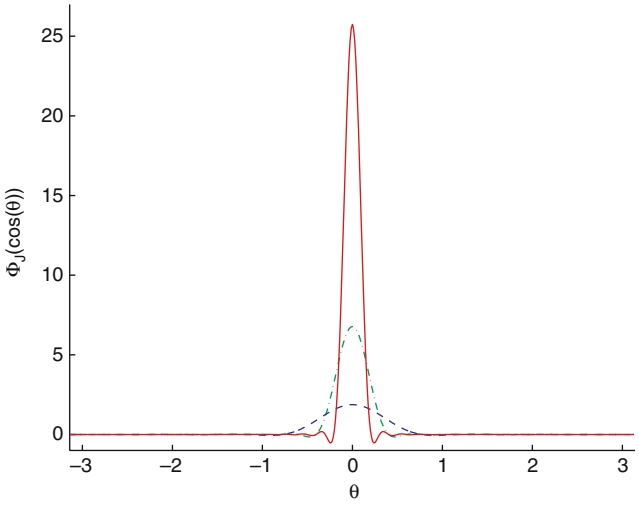

Fig. 1 Sectional plot of the cubic polynomial (CuP) scaling functions Φ_3, Φ_4 and Φ_5, respectively, illustrated by a dashed, dash-dotted and a solid line

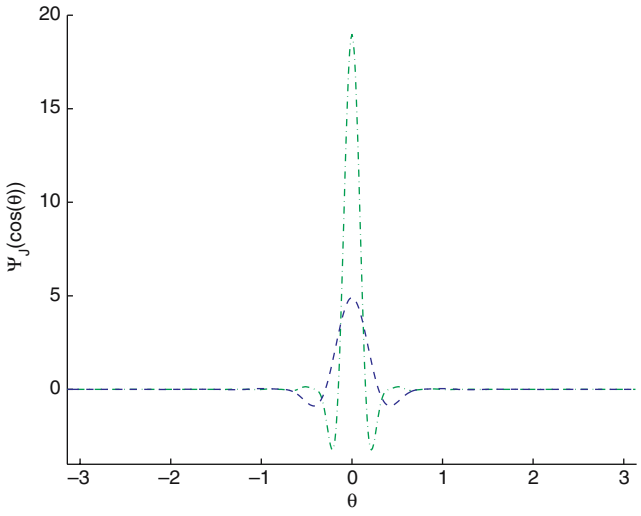

Fig. 2 Sectional plot of the CuP wavelets Ψ_3 and Ψ_4 illustrated by a dashed and a dash-dotted line

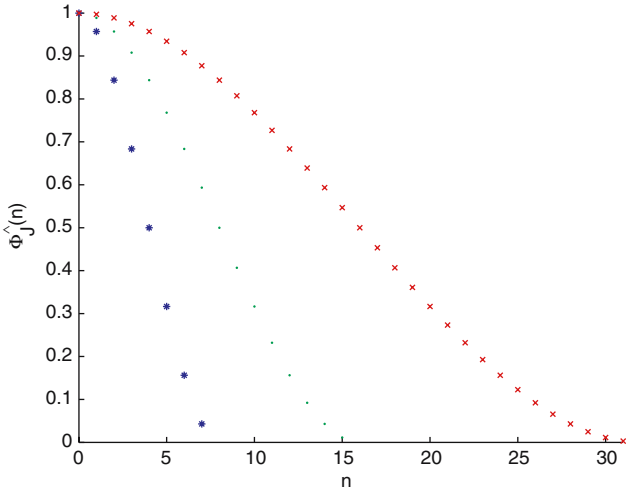

Fig. 3 Symbol of the CuP scaling functions Φ_3, Φ_4 and Φ_5, respectively, illustrated by star, dot and cross

of the scaling function and the wavelet are shown in Figs. 3 and 4.

Double convolution between a function $F \in L^2(\Omega)$ and a scaling function $\Phi_J(\eta,\cdot)$ yields the scale approximation $S_J(F)$ of scale J. More explicitly, we have

$$S_J(F) = \Phi_J * \Phi_J * F \tag{16}$$

$$= \int_\Omega \int_\Omega \Phi_J(\eta,\cdot)\Phi_J(\eta,\xi)F(\xi)\,\mathrm{d}S(\xi)\,\mathrm{d}S(\eta), \tag{17}$$

where $\mathrm{d}S(\eta)$ denotes the surface integral with integration variable η. The latter leads us immediately to the scale space

$$\mathcal{V}_J = \left\{ \Phi_J * \Phi_J * F \,\middle|\, F \in L^2(\Omega) \right\}. \tag{18}$$

In this context, the operator

$$W_J(F) = \tilde{\Psi}_J * \Psi_J * F \tag{19}$$

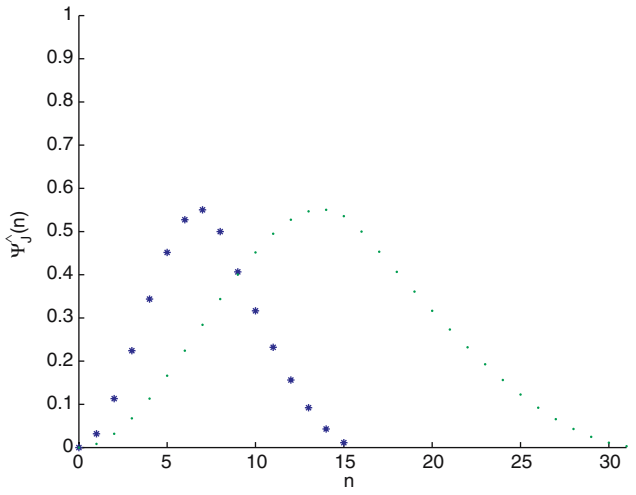

Fig. 4 Symbol of the CuP wavelets Ψ_3 and Ψ_4, illustrated by star and dot

yields the wavelet approximation of F at scale J and the detail space

$$\mathcal{W}_J = \left\{ \tilde{\Psi}_J * \Psi_J * F \,\middle|\, F \in L^2(\Omega) \right\}. \tag{20}$$

Whereas S_J acts as a low-pass filter, we can understand W_J as a band-pass filter. By construction, we obtain a multiresolution analysis satisfying

$$\mathcal{V}_0 \subset \cdots \subset \mathcal{V}_J \subset \mathcal{V}_{J+1} \subset \cdots \subset L^2(\Omega), \tag{21}$$

and

$$L^2(\Omega) = \overline{\bigcup_{J=0}^{\infty} \mathcal{V}_J}^{\|\cdot\|_{L^2(\Omega)}}. \tag{22}$$

Clearly, we can understand the convolution $(\Psi_J * F)(\eta)$ as a decomposition of F, which provides us with wavelet coefficients of scale J at some location $\eta \in \Omega$. Vice versa, we can interpret $\tilde{\Psi}_J * (\Psi_J * F)$ as a reconstruction of F from its wavelet coefficients. That is why we refer in the following to the *decomposition wavelet* Ψ_J and the *reconstruction wavelet* $\tilde{\Psi}_J$.

2.2 Wavelet variances

Once equipped with the wavelet coefficients of $F \in L^2(\Omega)$, one can derive a decomposition of the energy $\|F\|^2_{L^2(\Omega)}$ of a signal F in analogy to the well-known approach involving degree variances. To demonstrate the relationship between the two, we let

$$\mathrm{Var}_{n,k}(F) = F_{n,k}^2 = \left(\int_\Omega Y_{n,k}(\xi) F(\xi) \mathrm{d}S(\xi) \right)^2, \tag{23}$$

such that

$$\mathrm{Var}_n(F) = \sum_{k=-n}^{n} \mathrm{Var}_{n,k}(F) \tag{24}$$

denotes the degree variances. Mathematically speaking, the degree variances are a decomposition of the $L^2(\Omega)$-norm of F, i.e., we arrive at

$$\|F\|^2_{L^2(\Omega)} = \sum_{n=0}^{\infty} \mathrm{Var}_n(F). \tag{25}$$

In case of wavelet variances, we substitute the spherical harmonics by our localizing basis functions.

In detail, the dimensionless wavelet variances of scale $J \in \mathbb{N}_0$ and location η are given by

$$\mathrm{Var}_{J;\eta}(F) = \left(\int_\Omega \Psi_J(\xi, \eta) F(\xi) \mathrm{d}S(\xi) \right)^2 \tag{26}$$

$$= ((\Psi_J * F)(\eta))^2, \tag{27}$$

where $\eta \in \Omega$. Hence, we can interpret Eq. (27) as the regional energy content in the signal F located around $\eta \in \Omega$. To make this more evident, we let $\Psi_{-1} = \Phi_0$ and borrow from Freeden and Michel (2004) that

$$\|F\|^2_{L^2(\Omega)} = \sum_{J=-1}^{\infty} \int_\Omega \mathrm{Var}_{J;\eta}(F)\, \mathrm{d}S(\eta).$$

Due to their strong relation to the regional energy content of a signal, the wavelet variances provide an appropriate tool for a wavelet compression of the gravitational field data. Moreover, they can be used for (spatial) denoising procedures as proposed by Freeden and Maier (2002).

3 GRACE and hydrology data

The GRACE science team released over 20 monthly global Earth gravitational fields in terms of spherical harmonic coefficients (http://www.csr.utexas.edu/grace/gravity). They are – apart from some gaps – nearly continuous in time. We use 22 fields between April/May 2002 and July 2004. The coefficients are given up to spherical harmonic degree and order 120, except for January 2004 (up to 70) together with so-called "calibrated" error files.

In order to avoid aliasing effects of the high-frequency mass variations of tides and the atmospheric and oceanic circulation, their influence is already removed during the data processing using various models (see Bettadpur 2003). Under the assumption of error-free dealiasing models, most of the remaining monthly gravity anomalies are probably generated by hydrological mass redistributions.

Hydrological mass variations are the sum of water redistributions on the continents involving precipitation, evaporation, surface runoff, snow coverage, soil moisture and groundwater storage. There are different global models of these processes available. For this study we used the climate prediction center (CPC) model (Fan and van den Dool 2004) and the land dynamics (LaD) model (Milly and Shmakin 2002) in their current versions. While the CPC model covers

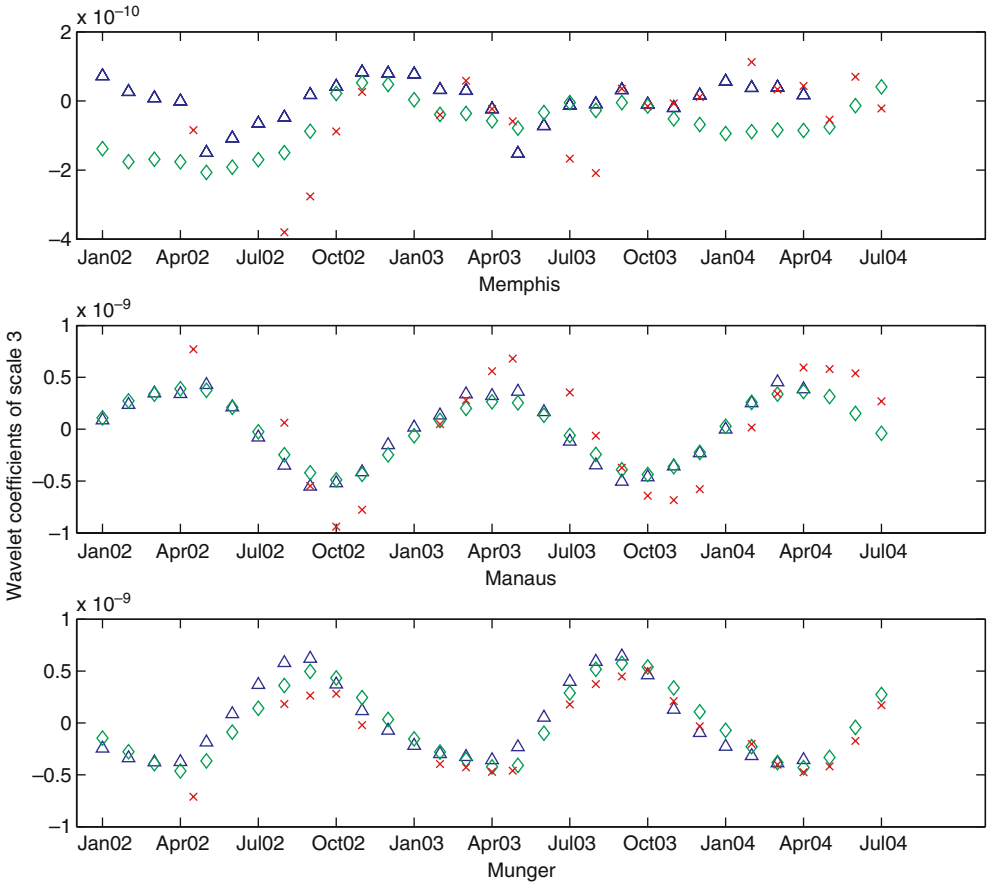

Fig. 5 Time-series of wavelet coefficients of scale 3 obtained from gravity recovery and climate experiment (GRACE; *cross*), climate prediction center (CPC; *open diamond*), land dynamics (LaD; *open triangle*) at Memphis (Tennessee), Manaus (Brazil), and Munger (India) during the months January 2002–July 2004

the whole considered time span, the LaD (release "LaD-World-Danube") model stops in April 2004.

4 Application to GRACE models

In case of GRACE, the gravitational potential V^{GRACE} is provided via dimensionless Fourier coefficients $\tilde{V}_{n,k}$ corresponding to fully normalized spherical harmonics. These spherical harmonics differ by a factor of $1/\sqrt{4\pi}$ from those introduced above. As proposed by Tapley et al. (2004b), terms of degree 0, 1 and 2 are omitted, since they show a special behavior (see Chen et al. 2004).

Exploiting the Fourier expansion, one obtains a representation of V^{GRACE} in $\mathcal{V}_J$ by

$$S_J\left(V^{\mathrm{GRACE}}\right)(t,x) = \left(\Phi_J * \Phi_J * V^{\mathrm{GRACE}}\right)(t,x) = \sqrt{4\pi}\frac{GM}{R}\sum_{n=3}^{120}\sum_{k=-n}^{n}\tilde{V}_{n,k}(t) \times (\Phi_J^{\wedge}(n))^2 Y_{n,k}\left(\frac{x}{|x|}\right), \tag{28}$$

where $x \in \Omega_R$, respectively, in the wavelet space $\mathcal{W}_J$ by

$$W_J\left(V^{\mathrm{GRACE}}\right)(t,x) = \sqrt{4\pi}\frac{GM}{R}\sum_{n=3}^{120}\sum_{k=-n}^{n}\tilde{V}_{n,k}(t) \times (\Psi_J^{\wedge}(n))^2 Y_{n,k}\left(\frac{x}{|x|}\right). \tag{29}$$

The latter representation provides us with the dimensionless wavelet coefficient at some location $y \in \Omega_R$, i.e.,

$$\frac{R}{GM}\left(\Psi_J * V^{\mathrm{GRACE}}\right)(t,x) = \sqrt{4\pi}\sum_{n=3}^{120}\sum_{k=-n}^{n}\tilde{V}_{n,k}(t) \times \Psi_J^{\wedge}(n) Y_{n,k}\left(\frac{x}{|x|}\right). \tag{30}$$

A time-series of wavelet coefficients computed by Eq. (30) is illustrated in Figs. 5 and 6.

For our study of the temporal variations, we subtract an annual mean gravitational potential V_{mean} of the fields computed from the months August 2003 to July 2004 (except for January 2004 since the potentials are error dominated). The problem of determining an annual mean is discussed in Kohlhaas (2005).

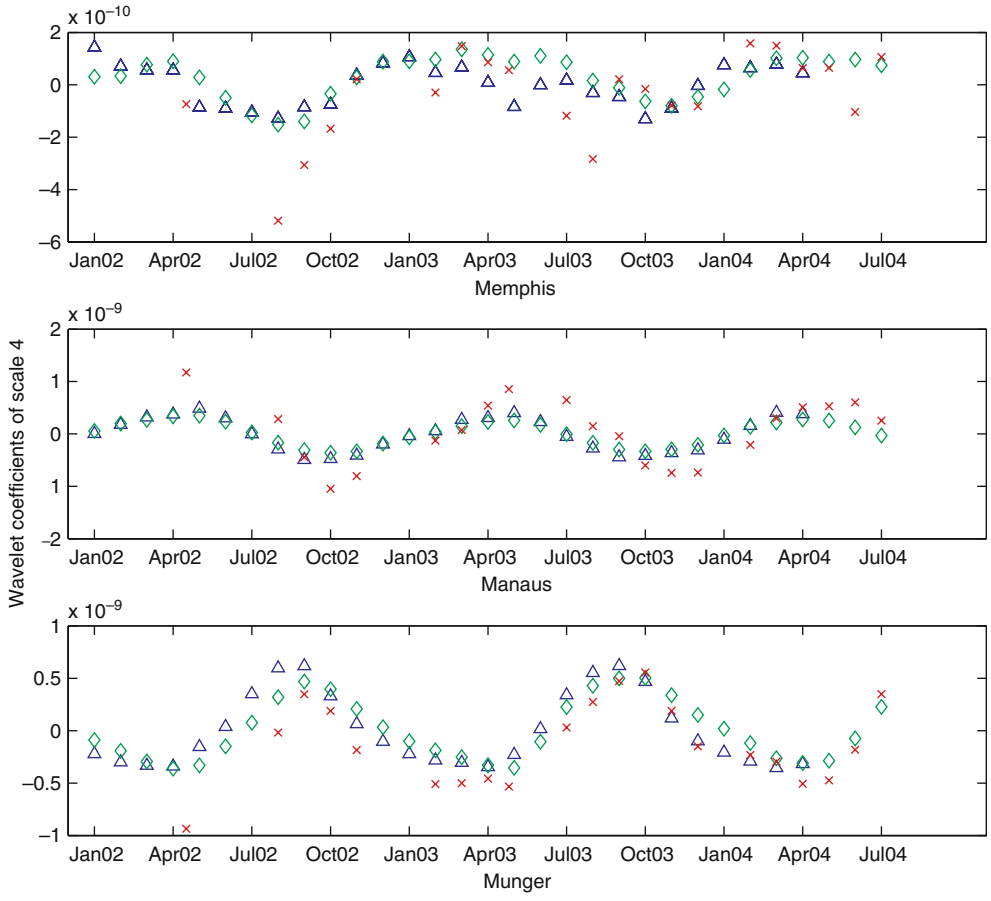

Fig. 6 Time-series of wavelet coefficients of scale 4 obtained from GRACE (*cross*), CPC (*open diamond*), LaD (*open triangle*) at Memphis (Tennessee), Manaus (Brazil), and Munger (India) during the months January 2002–July 2004

5 Application to hydrology models

We compute the gravitational variations ΔV^{Hyd} from surface density variations $\Delta\sigma$ provided by the LaD model and from water-column heights provided by the CPC model. Since the gravity variations discussed here are induced by variations in mass–density, we are concerned with $\Delta\rho(t,\cdot)$, which is of class $L^2(\Omega_R^{\mathrm{int}})$ for all times t. To ensure comparability with the GRACE gravity signal, we also remove all spectral terms of degree 0, 1 and 2 from $\Delta\rho(t,\cdot)$. Then

$$\Delta V^{\mathrm{Hyd}}(t,x) = G \int_{\Omega_R^{\mathrm{int}}} \frac{\Delta\rho(t,y)}{|x-y|}\,\mathrm{d}V(y), \quad x \in \Omega_R^{\mathrm{ext}}. \tag{31}$$

We borrow from Freeden et al. (1998) that

$$\frac{1}{|x-y|} = \frac{1}{|x|}\sum_{n=0}^{\infty}\left(\frac{|y|}{|x|}\right)^n P_n\left(\frac{x}{|x|}\cdot\frac{y}{|y|}\right). \tag{32}$$

Inserting Eq. (32) into Eq. (31), and interchanging the summation and integration we deduce

$$\Delta V^{\mathrm{Hyd}}(t,x) = \frac{G}{|x|}\sum_{n=0}^{\infty}\int_{\Omega_R^{\mathrm{int}}}\left(\frac{|y|}{|x|}\right)^n \Delta\rho(t,y) \times P_n\left(\frac{x}{|x|}\cdot\frac{y}{|y|}\right)\mathrm{d}V(y), \tag{33}$$

for $x \in \Omega_R^{\mathrm{ext}}$.

Following Wahr et al. (1998), we assume that the mass–density variations occur only in a thin layer of thickness $H \ll R$ close to the surface Ω_R. Understanding $\Delta\rho(t,\cdot)$ as pure spherical function $\Delta\hat{\rho}(t,\cdot) \in L^2(\Omega)$ and using the unique decomposition of $x \in \Omega_R^{\mathrm{ext}}$ into $x = |x|\xi$, $\xi \in \Omega$, we obtain

$$\begin{aligned}\Delta V^{\mathrm{Hyd}}(t,|x|\xi) &\approx \frac{G|x|^2}{|x|}\sum_{n=0}^{\infty}\int_{\Omega}\Delta\hat{\rho}(t,\eta)P_n(\xi\cdot\eta)\,\mathrm{d}S(\eta) \\ &\quad\times \underbrace{\int_{R-H}^{R}\left(\frac{r}{|x|}\right)^{n+2}\mathrm{d}r}_{\approx\frac{R^{n+2}}{|x|^{n+2}}H}\end{aligned} \tag{34}$$

$$\approx G|x| \sum_{n=0}^{\infty} \int_{\Omega} \frac{R^{n+2}}{|x|^{n+2}} \Delta\hat{\rho}(t,\eta) H P_n(\xi \cdot \eta)\, \mathrm{d}S(\eta). \quad (35)$$

Now, we introduce the quantity $\Delta\sigma(t,\eta) = \Delta\hat{\rho}(t,\eta)H$, which can be understood as a surface density [kg/m^2]. Extending the right-hand side by the Earth's mass $M = (4\pi R^3\overline{\rho})/3$, where $\overline{\rho}$ denotes the Earth's mean mass–density, we derive

$$\Delta V^{\mathrm{Hyd}}(t,|x|\xi) \approx \frac{GM}{R} \sum_{n=0}^{\infty} \int_{\Omega} \frac{R^{n+1}}{|x|^{n+1}} \frac{3}{4\pi\overline{\rho}R} \Delta\sigma(t,\eta) \times P_n(\xi \cdot \eta)\, \mathrm{d}S(\eta) \quad (36)$$

$$= \frac{GM}{R} \int_{\Omega} \sum_{n=0}^{\infty} \frac{R^{n+1}}{|x|^{n+1}} \frac{3}{4\pi\overline{\rho}R} \Delta\sigma(t,\eta) \times P_n(\xi \cdot \eta)\, \mathrm{d}S(\eta), \quad (37)$$

for $x \in \Omega_R^{\mathrm{ext}}$, where interchanging the infinite sum and integral is possible, since we have $\Delta\sigma(t,\cdot) \in L^2(\Omega_R^{\mathrm{int}}) \subset L^1(\Omega_R^{\mathrm{int}})$ for all $t \in \mathbb{R}$ by assumption.

We deal with mass variations on the Earth's surface, so we have to consider loading by taking the Love numbers into account. This leads us to

$$\Delta V^{\mathrm{Hyd}}(t,|x|\xi) = \frac{GM}{R} \int_{\Omega} \sum_{n=0}^{\infty} \frac{R^{n+1}}{|x|^{n+1}} \frac{3(1+k_n')}{4\pi\overline{\rho}R} \Delta\sigma(t,\eta) \times P_n(\xi \cdot \eta)\, \mathrm{d}S(\eta), \quad (38)$$

where k_n' denotes the load Love number. We use the values from Wahr et al. (1998).

Now we can compute the J-level approximation for the outer space. In the case of GRACE, we were even able to compute the potential on Ω_R. However, for the hydrology models, we need $x \in \Omega_R^{\mathrm{ext}}$ to interchange integral and sum. Since in our application potential (given on a grid), as well as scaling functions and wavelets, are bandlimited, we can also give an expression for the case $x \in \Omega_R$. For details about the J-level approximation in the outer space and the limit considerations, see Kohlhaas (2005). We arrive at

$$S_J\left(\Delta V^{\mathrm{Hyd}}\right)(t,x) = \frac{GM}{R} \int_{\Omega} \sum_{n=0}^{\infty} \frac{3(1+k_n')}{4\pi\overline{\rho}R} (\Phi_J^{\wedge}(n))^2 \times \Delta\sigma(t,\eta) P_n\left(\frac{x}{|x|} \cdot \eta\right) \mathrm{d}S(\eta) \quad (39)$$

for $x \in \Omega_R$.

Hence, we can rewrite the latter equation in terms of spherical convolutions by

$$S_J\left(\Delta V^{\mathrm{Hyd}}\right)(t,R\cdot) = \frac{GM}{R} \Phi_J * \frac{3}{\overline{\rho}R} \Phi_J^{\mathrm{L}} * \Delta\sigma(t,\cdot), \quad (40)$$

where Φ_J^{L} denotes the modified scaling function

$$\Phi_J^{\mathrm{L}}(\xi,\eta) = \sum_{n=0}^{\infty} \Phi_J^{\wedge}(n) \frac{1+k_n'}{4\pi} P_n(\xi \cdot \eta), \quad \xi,\eta \in \Omega. \quad (41)$$

The superscript L denotes its association with the Love numbers. The reconstruction scaling function Φ_J is defined as in Eq. (10). Analogously, we derive the representation in terms of spherical wavelets. Then

$$W_J\left(\Delta V^{\mathrm{Hyd}}\right)(t,R\cdot) = \frac{GM}{R} \tilde{\Psi}_J * \frac{3}{\overline{\rho}R} \Psi_J^{\mathrm{L}} * \Delta\sigma(t,\cdot), \quad (42)$$

where Ψ_J^{L} is defined in analogy to Φ_J^{L}.

The wavelet decomposition $\Psi_J^{\mathrm{L}} * \Delta\sigma$ is computed numerically since the data describing the surface mass–density, as well as the moisture, are only given on the continents. For the numerical integration, we choose a polynomially exact integrating, equiangular grid as proposed, e.g., by Driscoll and Healy (1994).

6 Numerical results

Since the variations of GRACE monthly mean gravity fields are known to be dominated by large seasonal continental mass variations, we give results for these phenomena using the method described above. The extrema of the variations occur in spring and autumn in each hemisphere. Figures 7 and 8 show the variations of the gravitational potential from GRACE relative to the mean in October 2003 (in direct comparison to Figs. 9, 10, 11 and 12 representing the gravitational signal computed from hydrology models). Figures 13 and 14 show the same for April 2004. The wavelet scales 3 and 4 are given. Roughly speaking, these scales correspond to the spherical harmonic degrees around 7 and around 14 (see Fig. 4).

Higher scales are not representative due to the increase of the GRACE errors with increasing degree (Tapley et al., 2004b; Wahr et al., 2004). At lower wavelet scales (e.g., 2 or less, which are not shown here) the wavelets take a large area into account (half of the globe or more). Consequently, these scales mix up oceanic with continental areas or even polar with equatorial regions. This is unfavorable when considering regional gravity variations. The influence of the farther distant surrounding decreases massively when considering higher frequency regional signals as it is shown in Figs. 7, 8, 9, 10, 11, 12, 13, 14, 15, 16, 17, and 18.

The largest variations show up for the well-known large drainage basins like the Amazon, the Congo, the Zambezi or the watershed of the Bay of Bengal (Ganges). A comparison between Southern and Northern Hemisphere reveals the shift in seasons. In April, the maximal deviations can be found in the Southern Hemisphere, while there are minima on the Northern Hemisphere. For October, the same holds the other way round.

Figures 9, 10, 15, 16, and 11, 12, 17 and 18 display the same quantities as in the case of GRACE for the LaD and the CPC model. The differences between the models and the differences relative to the GRACE gravity fields are due to inaccuracies in both; the GRACE gravity fields and the hydrology models.

In detail, the GRACE observations still contain unmodeled effects such as other remaining or neglected mass

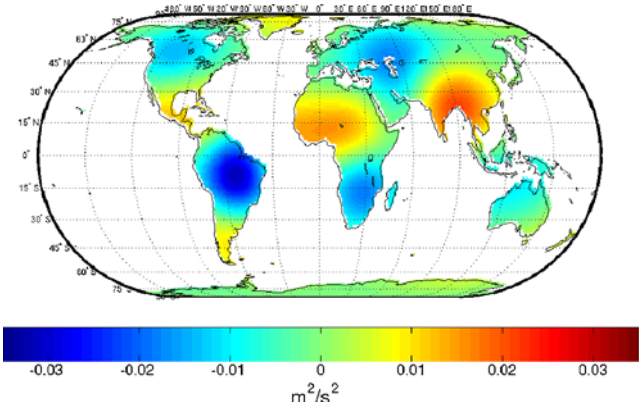

Fig. 7 Anomalies of the gravitational potential observed by GRACE at wavelet scale 3 in October 2003

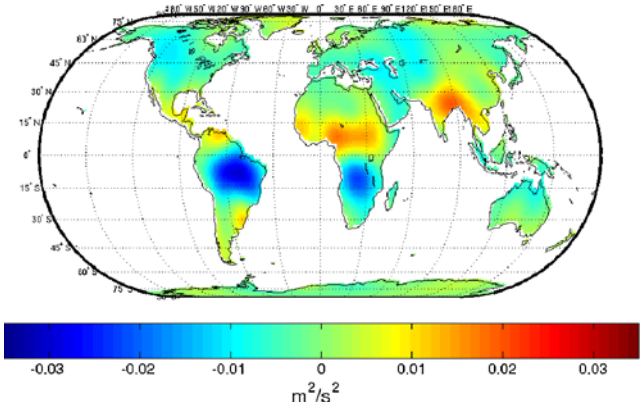

Fig. 8 Anomalies of the gravitational potential observed by GRACE at wavelet scale 4 in October 2003

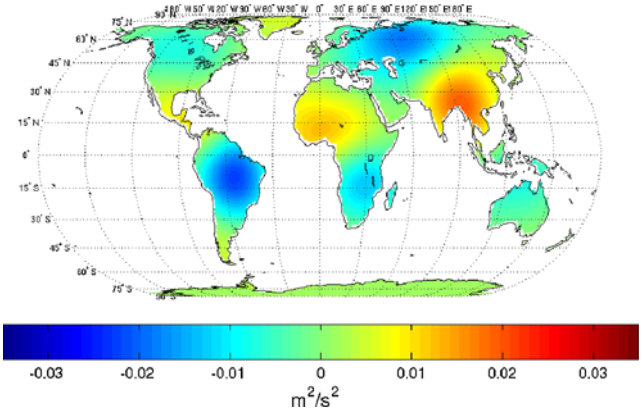

Fig. 9 Anomalies of the gravitational potential computed from land dynamics (LaD) model at wavelet scale 3 in October 2003

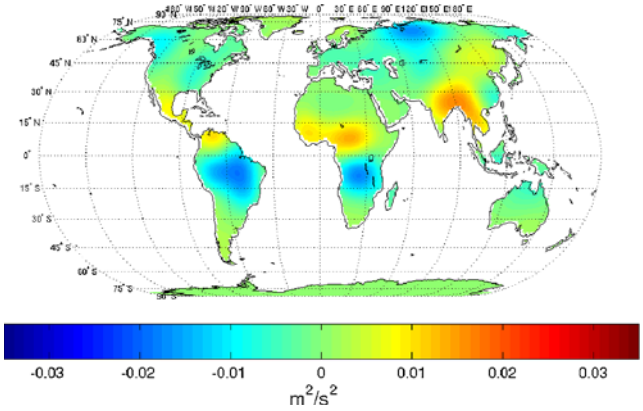

Fig. 10 Anomalies of the gravitational potential computed from LaD model at wavelet scale 4 in October 2003

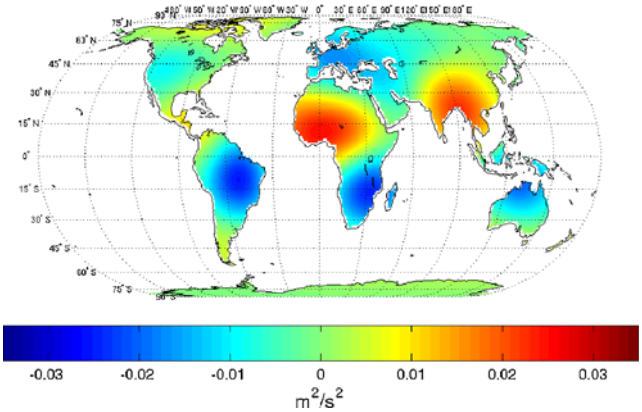

Fig. 11 Anomalies of the gravitational potential computed from CPC model at wavelet scale 3 in October 2003

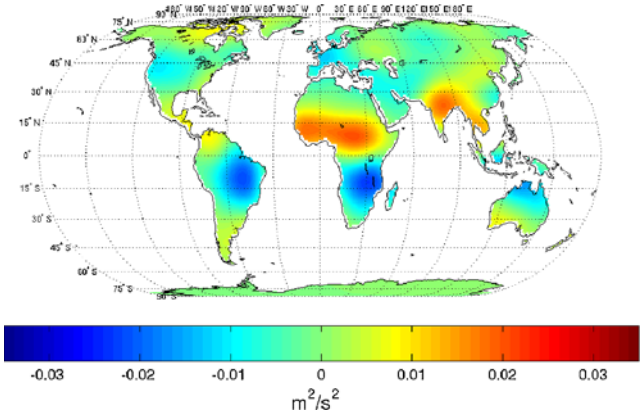

Fig. 12 Anomalies of the gravitational potential computed from CPC model at wavelet scale 4 in October 2003

redistributions, e.g., from ocean tides, in the atmosphere or from ice melting and post-glacial rebound, as well as GRACE instrument errors and shortcomings in the data processing. On the other hand, the deviations with and between the hydrology models can be due to irregularly distributed, heterogeneous and sometimes maybe erroneous input data, as well as mathematical approximations of physical processes. Therefore, we cannot expect a perfect agreement. For example, while the LaD model results in smaller amplitudes in general, the CPC model seems to underestimate the variations in the polar regions associated with accumulation and melting of snow. However, when focusing at typical drainage basins, quite a good agreement can be observed, which will be discussed below. For a closer look at the temporal evolution of the global variations, we refer to the electronic supplementary material (ESM) of this paper.

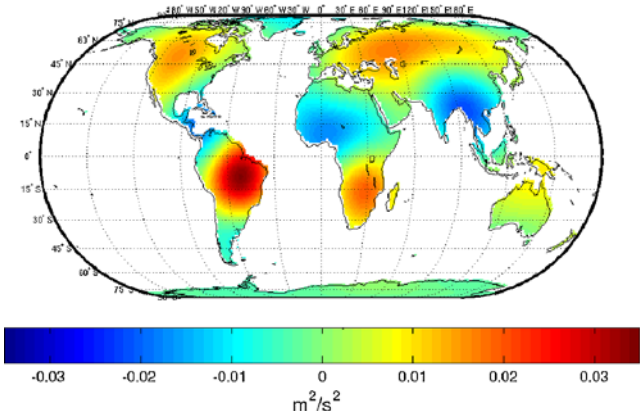

Fig. 13 Anomalies of the gravitational potential observed by GRACE at wavelet scale 3 in April 2004

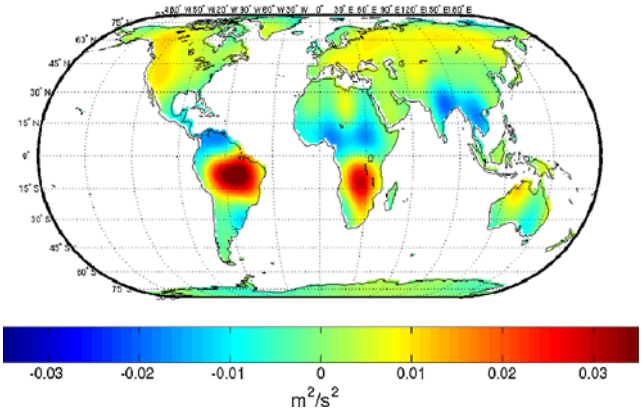

Fig. 14 Anomalies of the gravitational potential observed by GRACE at wavelet scale 4 in April 2004

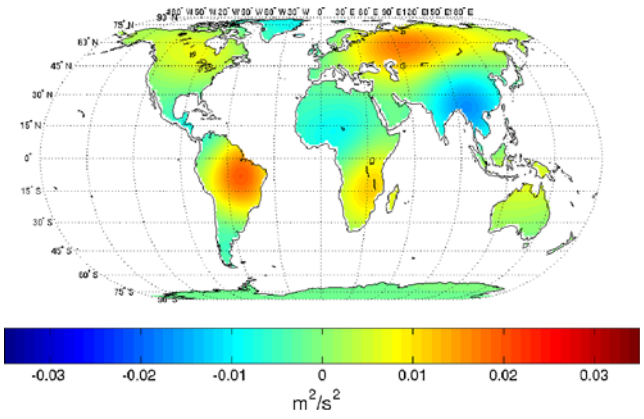

Fig. 15 Anomalies of the gravitational potential computed from LaD model at wavelet scale 3 in April 2004

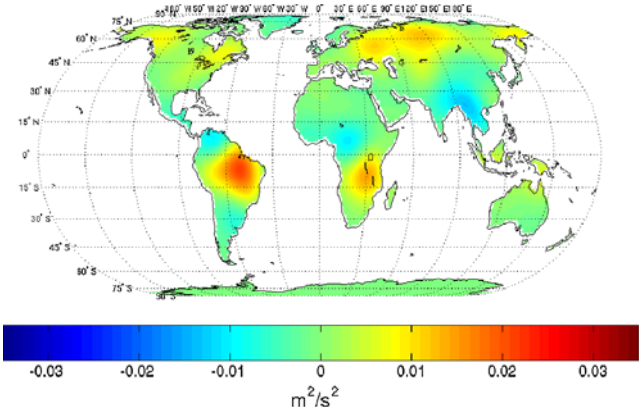

Fig. 16 Anomalies of the gravitational potential computed from LaD model at wavelet scale 4 in April 2004

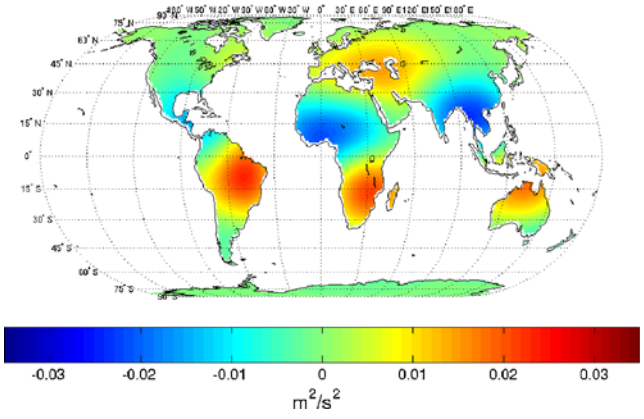

Fig. 17 Anomalies of the gravitational potential computed from CPC model at wavelet scale 3 in April 2004

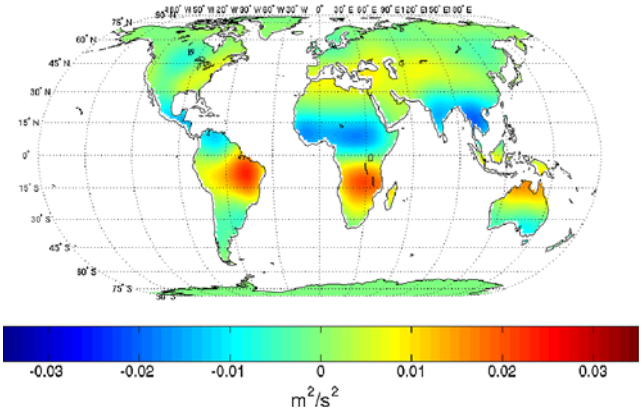

Fig. 18 Anomalies of the gravitational potential computed from CPC model at wavelet scale 4 in April 2004

A restriction to selected drainage basins can easily be obtained by looking at the time-series of the wavelet coefficients. Figures 5 and 6 give examples for the wavelet scales 3 and 4. Wavelet coefficients for Memphis (TN, USA), Manaus (Brazil) and Munger (India) representing the areas of the Mississippi, the Amazon and the watershed of the Bay of Bengal, respectively, were computed. In Manaus and Munger a seasonal signal is clearly dominant, while Memphis shows also some other unknown effect. The Mississippi area has a minor signal, which might be on the limit of detectability for GRACE. The time series also reveals a delay of the maximum of the signal between the GRACE data and the hydrology model prediction by approximately 1 month, which was already mentioned by Wahr et al. (2004).

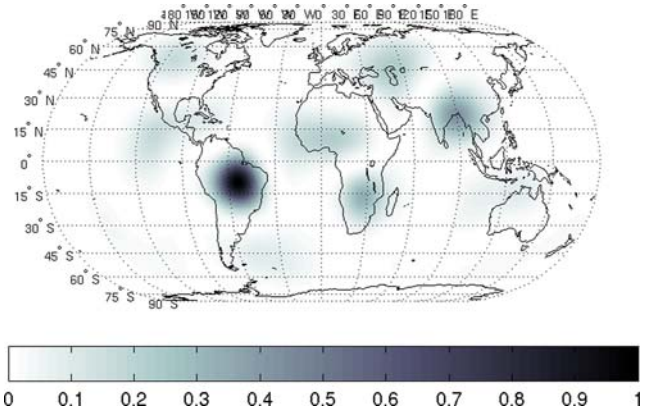

Fig. 19 GRACE wavelet variances of scale 3 in October 2003 (normalized)

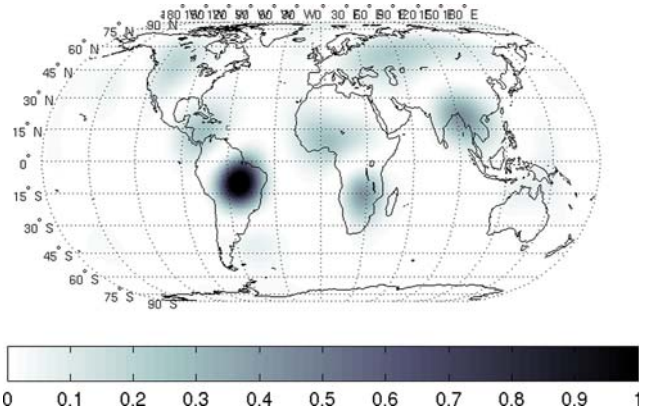

Fig. 20 GRACE wavelet variances of scale 3 in April 2004 (normalized)

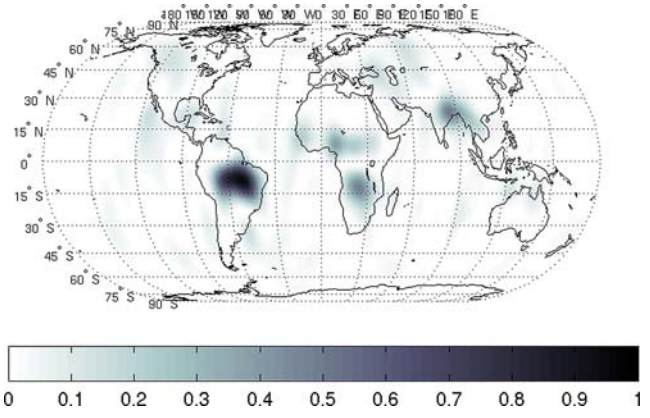

Fig. 21 GRACE wavelet variances of scale 4 in October 2003 (normalized)

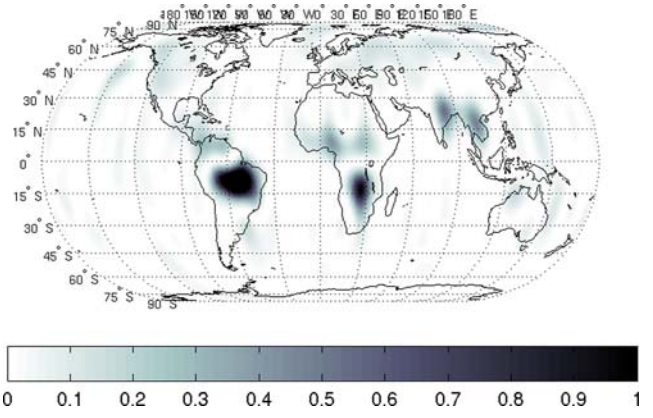

Fig. 22 GRACE wavelet variances of scale 4 in April 2004 (normalized)

The agreement between the GRACE observations and the hydrology models is very impressive. This is evident when looking at correlation coefficients between the time series illustrated in Figs. 5 and 6. In particular, we obtain in Tables 1, 2 and 3 that the GRACE signal is highly correlated to the hydrology signal. Again, the CPC model performs best in the Bay of Bengal. Also, the Amazon basin yields high correlations for both models, while the Mississippi is worse. Still, the numbers are excellent when comparing with the spatial coefficients computed by Andersen and Hinderer (2005) for interannual gravity variations.

Finally, we illustrate in Figs. 19, 20, 21 and 22 the dimensionless wavelet variances for scale 3 and 4 in October 2003 and April 2004. Obviously, the wavelet variances characterize the regional energy content in the signal. This is in contrast to the well-known degree variances, which do not enable an interpretation of any regional change of energy.

7 Concluding remarks

In this work, we analyze the Earth's gravitational potential given in terms of spherical harmonic coefficients. We give the methodology for deriving wavelet expansions from these coefficients and from gridded data on a sphere using CuP wavelets. In a numerical application with the GRACE gravity fields and hydrology model output, we observe seasonal variations in the wavelet coefficients. The wavelet coefficients show strong correlations with the gravitational signal computed from the output of the hydrological models LaD and CPC (see Tables 1, 2, 3).

This correlation also becomes visible in the spatial domain. The wavelet scales 3 and 4 are the most suited scales for this analysis, since they fit best with the spatial extension of the investigated phenomena. The numerical results are similar and in agreement to those obtained in previous studies (see e.g., Tapley et al. 2004b; Wahr et al. 2004); more details can be found in Kohlhaas (2005). This shows that wavelets are an appropriate tool to investigate regional and temporal variations in the Earth's gravitational field.

Since the point of departure in this study is the monthly GRACE gravity fields provided by the GRACE science team, no higher temporal resolution could be obtained. Recent studies showed that starting from the original GRACE observations the temporal resolution of the gravity variations could be increased regionally (Han et al. 2005a,b; Rowlands et al.

Table 1 Correlation coefficients for the time-series of the wavelet coefficients between GRACE and hydrology

Wavelet Scale 2	Memphis	Manaus	Munger
CPC	0.46	0.91	0.95
LaD	0.54	0.83	0.91

Table 2 Correlation coefficients for the time-series of the wavelet coefficients between GRACE and hydrology (see Fig. 5)

Wavelet Scale 3	Memphis	Manaus	Munger
CPC	0.54	0.88	0.97
LaD	0.52	0.81	0.90

Table 3 Correlation coefficients for the time-series of the wavelet coefficients computed between GRACE and hydrology (see Fig. 6)

Wavelet Scale 4	Memphis	Manaus	Munger
CPC	0.73	0.82	0.91
LaD	0.67	0.77	0.76

2005) at least by a factor of 2. Consequently, as a next step, it would be of interest to use the proposed wavelets for a direct gravity computation from GRACE observations with the intention of a high temporal and spatial resolution.

Acknowledgements We are thankful to the authors of the hydrology models at the Climate Prediction Center of NOAA and the US Geological Survey (USGS) for providing the hydrology data and to the GRACE science team and CSR-UT for providing the GRACE monthly gravity fields. Moreover, we gratefully acknowledge the financial support by the Forschungsschwerpunkt "Mathematik und Praxis", and the Graduiertenkolleg "Mathematik und Praxis" of the University of Kaiserslautern.

References

Andersen OB, Hinderer J (2005) Global inter-annual gravity changes from GRACE: early results. Geophys Res Lett 32:L01402. DOI 10.1029/2004GL020948

Bettadpur S (2003) Level-2 gravity field product user handbook, GRACE 327–734. CSR Publication no. GR-03-01, University of Texas, Austin

Chen JL, Wilson CR, Tapley BD, Ries JC (2004) Low degree gravitational changes from GRACE: validation and interpretation. Geophys Res Lett 31:L22607. DOI 10.1029/2004GL021670

Driscoll JR, Healy Jr DH (1994) Computing fourier transforms and convolutions on the 2-sphere. Adv Appl Math 15:202–250

Edmonds AR (1964) Drehimpulse in der Quantenmechanik. Bibliograph Inst, Mannheim

Fan Y, van den Dool H (2004) Climate prediction center global monthly soil moisture data set at 0.5° Resolution for 1948 to present. J Geophys Res 109:D10102. DOI 10.1029/2003JD004345

Fengler MJ (2005) Vector spherical harmonic and vector wavelet based non-linear Galerkin schemes for solving the incompressible Navier-Stokes equation on the sphere. University of Kaiserslautern, Department of Mathematics, Geomathematics Group, Shaker-Verlag, ISBN3-8322-4558

Fengler MJ, Freeden W, Gutting M (2004a) Darstellung des Gravitationsfeldes und seiner Funktionale mit sphärischen Multiskalentechniken. Zeitschrift für Geodäsie, Geoinformation und Landmanagement (ZfV) 129(5):323–334

Fengler MJ, Freeden W, Michel V (2004b) The Kaiserslautern multiscale geopotential model SWITCH-03 from orbit perturbations of the satellite CHAMP and its comparison to the models EGM96, UCPH2002_02_0.5, EIGEN-1s, and EIGEN-2. Geophys J Int 157:499–514, DOI 10.1111/j.1365-246X.2004.02209.x

Freeden W (1999) Multiscale modelling of spaceborne geodata. BG Teubner, Stuttgart

Freeden W, Maier T (2002) On multiscale denoising of spherical functions: basic theory and numerical aspects. ETNA 14:40-62.

Freeden W, Michel V (2004) Multiscale potential theory (with applications to earth's sciences). Birkhäuser Verlag, Boston

Freeden W, Schreiner M (1995) Non-orthogonal expansions on the sphere. Math Methods Appl Sci 18:83–120

Freeden W, Windheuser U (1996) Spherical wavelet transform and its discretization. Adv Comput Math 5:51–94

Freeden W, Gervens T, Schreiner M (1998) Constructive approximation on the sphere (with applications to geomathematics). Clarendon, University Press Oxford

Han SC, Shum CK, Braun A (2005a) High-resolution continental water storage recovery from low–low satellite-to-satellite tracking. J Geodyn 39(1):11–28

Han SC, Shum CK, Jekeli C, Alsdorf D (2005b) Improved estimation of terrestrial water storage changes from GRACE. Geophys Res Lett 32:L07302. DOI 10.1029/2005GL022382

Jekeli C (1981) Alternative methods to smooth the earth's gravity field. Report 327, Department of Geodetic Science Survey, Ohio State University, Columbus

Kohlhaas A (2005) Multiscale modelling of temporal and spatial variations in the earth's gravity potential observed by GRACE. Diploma Thesis, Geomathematics Group, Department of Mathematics, University of Kaiserslautern

Maier T (2003) Multiscale geomagnetic field modelling from satellite data. PhD Thesis, Geomathematics Group, Department of Mathematics, University of Kaiserslautern

Mayer C (2003) Wavelet modelling of ionospheric currents and induced magnetic fields from satellite data. PhD Thesis, Geomathematics Group, Department of Mathematics, University of Kaiserslautern

Milly PCD, Shmakin AB (2002) Global modeling of land water and energy balances. Part I: The land dynamics (LaD) Model. J Hydrometeorol 3:283–299

Ramillien G, Cazenave A, Brunau O (2004) Global time variations of hydrological signals from GRACE satellite gravimetry. Geophys J Int 158:813–826. DOI 10.1111/j.1365-264X.2004.02328.x

Rowlands DD, Luthcke SB, Klosko SM, Lemoine FGR, Chinn DS, McCarthy JJ, Cox CM, Andersen OB (2005) Resolving mass flux at high spatial and temporal resolution using GRACE intersatellite measurements. Geophys Res Lett 32:L04310. DOI 10.1029/2004GL021908

Swenson S, Wahr J (2002) Methods for inferring regional surface-mass anomalies from gravity recovery and climate experiment measurements of time-variable gravity. J Geophys Res 107(B9):2193. DOI 10.1029/2001JB000576

Swenson S, Wahr J, Milly PCD (2003) Estimated accuracies of regional water storage variations inferred from the gravity recovery and climate experiment (GRACE). Water Resour Res 39(8):1223. DOI 10.1029/2002WR001808

Tapley BD, Bettadpur S, Watkins MM, Reigber C (2004a) The gravity recovery and climate experiment: mission overview and early results. Geophys Res Lett 31:L09607. DOI 10.1029/2004GL019920

Tapley BD, Bettadpur S, Ries JC, Thompson PF, Watkins MM (2004b) GRACE measurements of mass variability in the Earth system. Science 305:503–505

Wahr J, Molenaar M, Bryan F (1998) Time variability of the Earth's gravity field: hydrological and oceanic effects and their possible detection using GRACE. J Geophys Res 103(B12):30205–30229

Wahr J, Swenson S, Zlotnicki V, Velicogna I (2004) Time-variable gravity from GRACE: first results. Geophys Res Lett 31:L11501. DOI 10.1029/2004GL019779